ETH zürich

ETH Library

Line-Broadening in Low-Temperature Solid-State NMR Spectra of Fibrils

Journal Article

Author(s):
Bauer, Thomas; Dotta, Claudio; Balacescu, Livia; Gath, Julia; Hunkeler, Andreas; Böckmann, Anja; Meier, Beat H.

Publication date:
2017-01

Permanent link:
https://doi.org/10.3929/ethz-b-000128542

Rights / license:
In Copyright - Non-Commercial Use Permitted

Originally published in:
Journal of Biomolecular NMR 67(1), https://doi.org/10.1007/s10858-016-0083-4

Funding acknowledgement:
159707 - NMR studies in the Solid State (SNF)
146757 - NMR studies in the Solid State (SNF)

This page was generated automatically upon download from the ETH Zurich Research Collection.
For more information, please consult the Terms of use.

J Biomol NMR (2017) 67:51–61
DOI 10.1007/s10858-016-0083-4

ARTICLE

Line-Broadening in Low-Temperature Solid-State NMR Spectra of Fibrils

Thomas Bauer[1] · Claudio Dotta[1] · Livia Balacescu[1] · Julia Gath[1] · Andreas Hunkeler[1] · Anja Böckmann[2] · Beat H. Meier[1]

Received: 5 October 2016 / Accepted: 15 December 2016 / Published online: 4 February 2017
© Springer Science+Business Media Dordrecht 2017

Abstract The temperature-dependent resonance-line broadening of HET-s(218–289) in its amyloid form is investigated in the range between 110 K and 280 K. Significant differences are observed between residues in the structured hydrophobic triangular core, which are broadened the least and can be detected down to 100 K, and in the solvent-exposed parts, which are broadened the most and often disappear from the observed spectrum around 200 K. Below the freezing of the bulk water, around 273 K, the protein fibrils are still surrounded by a layer of mobile water whose thickness decreases with temperature, leading to drying out of the fibrils.

Keywords Solid-state NMR · Low-temperature · Line broadening · Fibrils · Protein · HET-s

Introduction

Solid-state NMR is the primary method for atomic-resolution structure determination of amyloid fibrils (Wasmer et al. 2008; van Melckebeke et al. 2010; Lu et al. 2013; Shi et al. 2015; Tuttle et al. 2016; Colvin et al. 2016; Wälti et al. 2016). However, its inherently low sensitivity sometimes limits its applicability to complex systems. If the line widths observed in NMR spectroscopy were temperature independent, the sensitivity could be increased by lowering the sample temperature, thereby exploiting beneficial factors such as a higher Boltzmann polarization and a lower thermal noise. With the application of dynamic nuclear polarization (DNP), one could even gain further in the signal-to-noise ratio, up to a factor of 660. (Can et al. 2015) Unfortunately, starting at the freezing temperature of the solvent water, one typically observes a significant broadening of the protein resonances (Linden et al. 2011; Siemer et al. 2012). This effect compromises most benefits of an increased signal strength. Nevertheless, successful DNP studies of amyloid fibrils were reported. (Debelouchina et al. 2010; Bayro et al. 2011; Debelouchina et al. 2013; Nagaraj et al. 2016).

The process leading to line broadening in proteins is not yet fully understood. One mechanism involved is the freezing out of motional processes between conformations with similar energy (Henzler-Wildman and Kern 2007) which are then observed separately, leading to heterogeneous line broadening (Linden et al. 2011). Above 200 K it has been observed that proteins retain a significant amount of liquid-like water around them which stays mobile long after the freezing of the bulk solvent in the sample (Siemer and McDermott 2008; Siemer et al. 2010, 2012). The conservation of this mobile water layer might have an influence on the line-broadening behavior observed, in particular for the solvent-exposed residues. A further mechanism is the presence of motion with correlation times corresponding to the inverse MAS or rf frequency, or intermediate chemical exchange between conformations. (Bajaj et al. 2009).

Electronic supplementary material The online version of this article (doi:10.1007/s10858-016-0083-4) contains supplementary material, which is available to authorized users.

✉ Anja Böckmann
a.bockmann@ibcp.fr

✉ Beat H. Meier
beme@ethz.ch

[1] Physical Chemistry, ETH Zurich, Vladimir-Prelog-Weg 2, CH-8093 Zurich, Switzerland

[2] Institut de Biologie et Chimie des Protéines, UMR 5086 CNRS, Université de Lyon 1, 7 passage du Vercors, 69367 Lyon, France

The typically monotoneous increase of the linewidth with decreasing temperature however indicates that the former machanisme is dominant in proteins. In this work, we observe and analyse the total linebroadening.

The model system used for this study consists of amyloid fibrils from the prion domain of HET-s, HET-s(218–289), from the filamentous fungus *Podospora anserina*. HET-s is a functional amyloid and induces a phenomenon known as heterokaryon incompatibility, which is a mechanism of self/non-self recognition that prevents a merging of genetically incompatible fungal colonies by the induction of cell death (Glass and Dementhon 2006; Saupe 2011).

The structure of HET-s(218–289) has been determined by solid-state NMR. It is described by a long β-solenoid with two windings formed from one monomer (Wasmer et al. 2008; van Melckebeke et al. 2010). The amino-acid sequence with arrows that indicate the position of the β-strands is shown in Fig. 1c. Schematically, the fibril is described by a long cylinder (typically micrometers long) with a hydrophobic center and partially charged and mainly hydrophilic surface in contact with water as shown in Fig. 1b. The only non-hydrophobic residues in the core are the polar residues threonine 233 and serine 273, which assist in the stabilization of the turn between two β-sheets by the formation of side-chain hydrogen bonds. All other polar or charged residues face to the outside of the fibril and are mostly located in solvent-accessible areas. The two windings of β-strands are interconnected via a more flexible

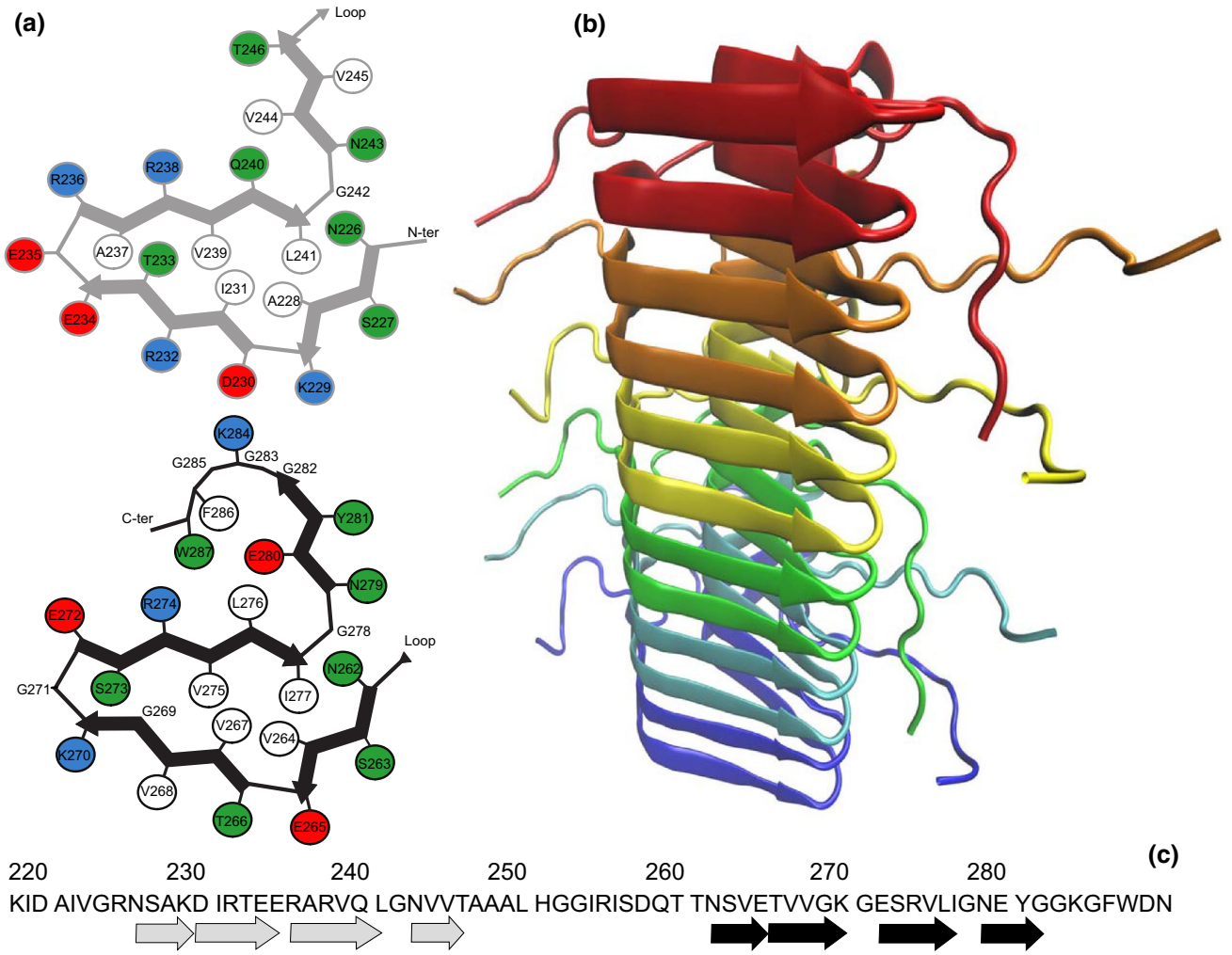

Fig. 1 **a** Schematic representation of the structure of HET-s(218–289) fibrils (Protein Data Bank ID 2KJ3). Eight β-sheets are forming two windings (*grey* and *black*) of a β-solenoid. The fibrils consist of a clearly structured triangular hydrophobic core, solvent-exposed residues and more flexible turn regions. Residues are color coded as follows *white, hydrophobic blue* and *red*, positively and negatively charged; green, polar. **b** A fibrillar stack of six consecutive individual molecules (*indicated by changing color*), which are formed by the two windings. **c** Amino-acid sequence of the prion domain of HET-s(218–289) excluding the histidine tag at the C-terminus. *Arrows* are indicating regions of β-sheet folds.(Wasmer et al. 2008; van Melckebeke et al. 2011)

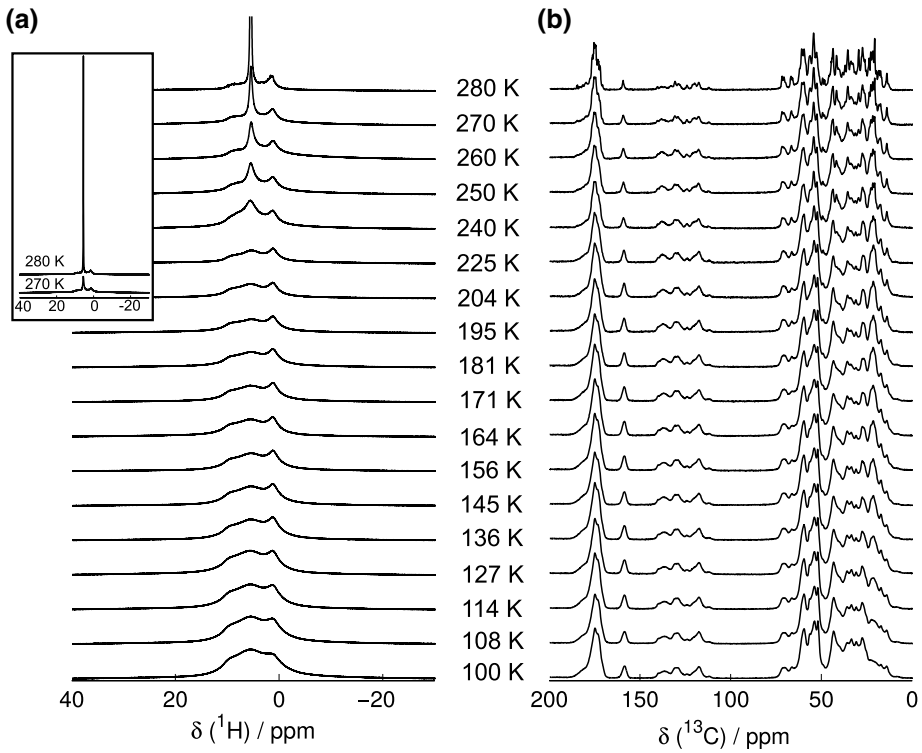

Fig. 2 **a** Proton spectra of HET-s(218–289) at temperatures between 100 and 280 K with an *inset* that shows the drop of water signal between the non-frozen and frozen state. With the freezing of the bulk water, the intensity of the mobile water signal drops immediately to roughly 30% of the initial value (signal integral). The lowering temperature causes the mobile water content to steadily decrease until the water becomes unobservable around 220 K. **b** ^{13}C cross polarization spectra of HET-s(218–289). An increasing line broadening of the one-dimensional spectrum with decreasing temperature is observed. Experimental details are given in Table S1

loop region. Previous studies have given a detailed picture of the solvent accessibility of the individual residues in the fibril (van Melckebeke et al. 2011). Basically all outward-facing residues are solvent exposed and the corresponding exchangeable sidechain protons show chemical exchange with water (Lesage and Böckmann 2003; van Melckebeke et al. 2011).

At temperatures significantly below freezing, a liquid water component remains in protein samples and has been observed for various types of proteins such as spider silk, SH3, Ubiquitin, Crh, and for anti-freeze proteins (van Beek et al. 1999; Lesage et al. 2008; Siemer et al. 2010, 2012; Linden et al. 2011).

Materials and methods

Sample preparation

[^{13}C,^{15}N] uniformly labeled HET-s(218–289) was expressed as described in (Balguerie et al. 2003). The fibrillization was performed in H_2O at pH 7.5 and 10 mM Cu(II)-EDTA was added to shorten T_1-relaxation times (Wickramasinghe et al. 2009). The protein was filled into a Bruker 1.3 mm MAS rotor via ultracentrifugation for 45 min in a Beckmann Coulter Optima L-90K centrifuge at 134,000 g using a home-made filling device (Böckmann et al. 2009).

Spectroscopy

All measurements were then carried out on a Bruker AVANCE III wide-bore spectrometer at a proton resonance frequency of 600 MHz. A Bruker 1.3 mm low temperature MAS probe with a temperature range from 100 K to room temperature was used in combination with a Bruker LT-MAS Cooling System for bearing, drive and sample cooling air. The temperature was calibrated with a sample of KBr powder (Thurber and Tycko 2009). All experiments were carried out at an MAS spinning frequency of 40 kHz. The cross-polarization field strengths were adjusted to 100 kHz on protons and 60 kHz on carbon. An adiabatic passage was used with a tangential shape on the proton channel with Δ_{rf} = 40 kHz and a contact time of 500 µs (Hediger et al. 1995; Ernst and Meier 2010). During the acquisition, XiX proton decoupling was applied at a field strength of 100 kHz (Tekely et al. 1994; Detken et al. 2002). The ^{13}C homonuclear correlation experiments used the DREAM sequence (Verel et al. 2001) with Δ_{rf} = 16 kHz. DREAM is an efficient first-order recoupling sequence that works well at 40 kHz spinning, where DARR-transfer is already severly attenuated. The decoupling strength was increased to 170 kHz during the DREAM period of 4 ms. The maximum t_1 and t_2 times were 10 and 15 ms, respectively, the interscan delay 3 s. A summary of acquisition and processing parameters is given in Table S1 in the supplementary material.

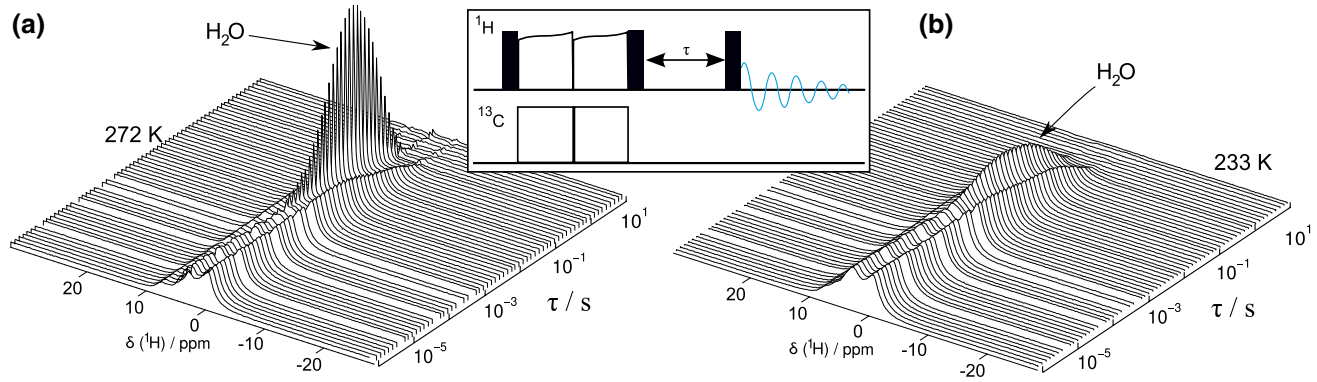

Fig. 3 Chemical exchange between the protein protons and its mobile water layer shown at 272 K and 233 K. After a double CP step (see *inset*) only protein polarization remains for $\tau=0$ and the water signal builds up during τ due to chemical exchange with the protein sidechains followed by spin diffusion. With the shrinking of the mobile water layer towards lower temperatures less returning signal is observed. After long enough waiting times relaxation leads to a decay of all observed resonances

Results

A significant amount of the total mass of a solid-state protein sample at ambient temperature consists of mobile, liquid-like water. For the highly viscous fibrillar HET-s(218–289) sample prepared by sedimentation in an ultracentrifuge, the water component amounts to around 75% of the total sample mass as determined by the weight loss upon lyophilization. In general, upon application of MAS, which leads to centrifugation with over $10^6 \times g$ (Böckmann et al. 2015) two water pools can be distinguished (Böckmann et al. 2009): a supernatant pool in the center of the rotor, and a pool of water interacting with the protein. For the samples described here, the supernatant pool was minimized in mass by using a high

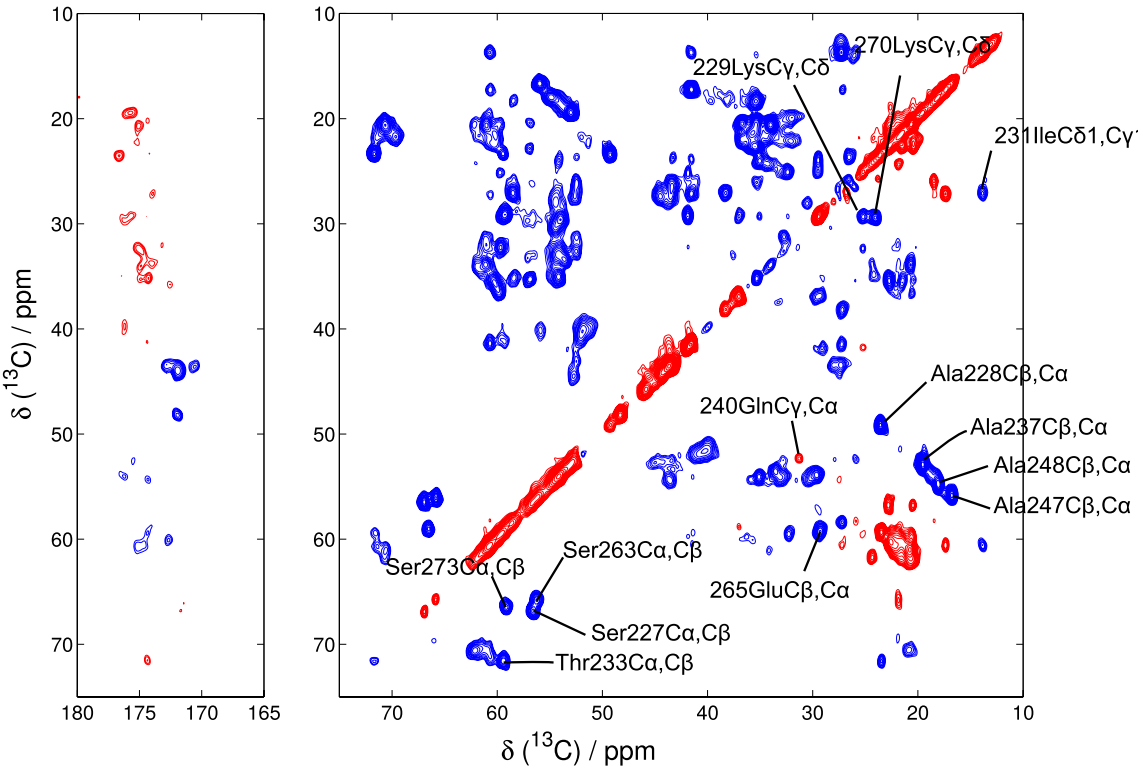

Fig. 4 Carbonyl and aliphatic regions of a DREAM spectrum of HET-s(218–290) at room temperature and 40 kHz MAS. The figure contains the labels for the cross peaks that have been evaluated in more detail during this study

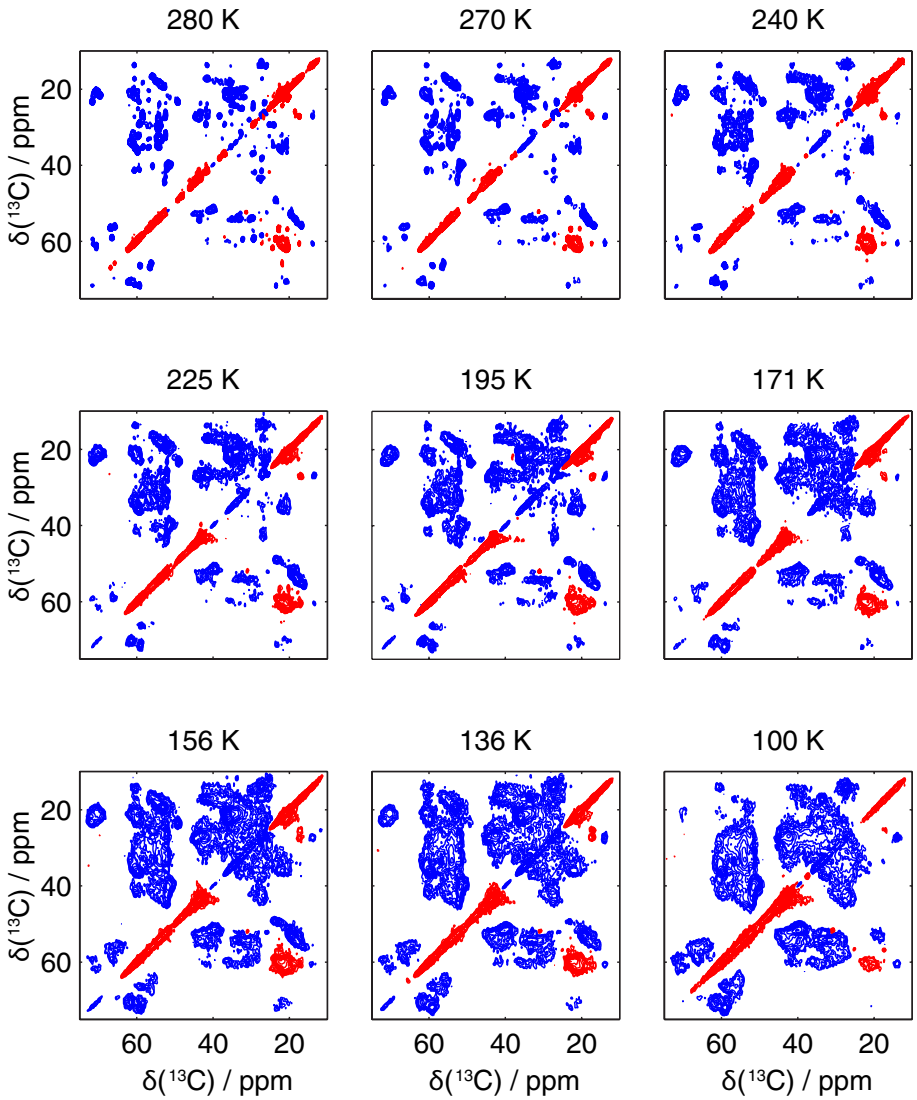

Fig. 5 DREAM spectra of HET-s(218–289) at different temperatures illustrating the general tendency of the resonances to broaden with decreasing temperature. Experimental details are listed in Figure S1

centrifugation frequency and prolonged sedimentation times during rotor filling (see "Materials and methods").

Figure 2a shows the one-dimensional proton spectra of HET-s(218–289) for temperatures between 280 and 100 K. The total signal is a superposition of the protein and the water proton resonances. Between room temperature and 270 K (enlarged in the inset) the signal intensity of water reduces drastically with the freezing of the bulk solvent. However, the mobile water component does not vanish entirely. Although the remaining water signal is hard to separate from the protein signal, one can estimate that the remaining integrated signal still adds up to roughly 30% of that at room temperature even if the peak amplitude of the water signal reduces by 91%. The signal of ice, with its large dipolar couplings, is too broad to be detected in Fig. 2. The remaining mobile water is in direct contact with the protein as demonstrated by the presence of chemical exchange between the protein (via exchangeable sidechains) and the liquid water: proton magnetization was prepared on the protein exclusively using a cross-polarization filter shown in the inset of Fig. 3 and the growing back of the water resonance in the mixing time τ, due to chemical exchange with the protein sidechains, was observed on a millisecond to second timescale (Lesage and Böckmann 2003; Lesage et al. 2008; van Melckebeke et al. 2011). The remaining protein signal and the growing in of a water line are detected via proton NMR as shown in Fig. 3. The water resonance reached its maximum intensity after 60 ms at 272 K. Finally, T_1 relaxation leads to a decay of all resonances. The strong water line appearing proofs that the liquid water is in contact with the protein. With decreasing temperature, the amount of mobile water gradually decreases and its resonance broadens until it becomes difficult to distinguish the water signal from the protein signal at around 220 K. The results at 233 K, in Fig. 3b, still show chemical exchange even at this temperature. The

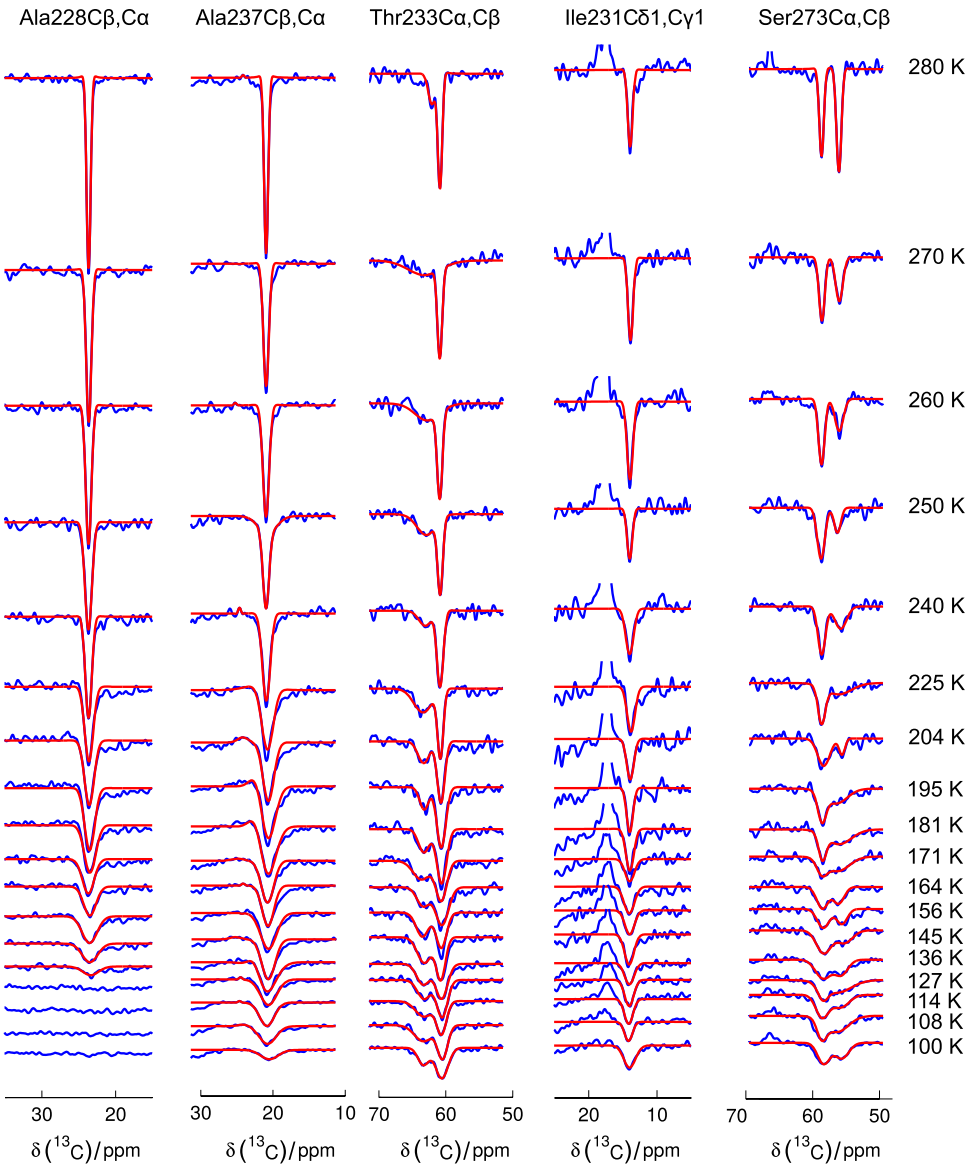

Fig. 6 1D slices from the 2D spectra of Fig. 5 (direct dimension) are given in *blue lines* and the best fit to the data as *red line*. All residues shown in this figure point to the inside of the fibril (see Fig. 1) and show a noticeable resilience against line broadening. The fits have been omitted where not meaningful anymore

peak maximum is reached after 20 ms. A fit of the water buildup and decay curves shows characteristic buildup and decay times of 20 and 390 ms at 272 K and 8 and 550 ms at 233 K. Here the buildup corresponds to the chemical exchange process, the decay to T_1 relaxation.

One-dimensional ^{13}C CP-MAS spectra as a function of temperature are given in Fig. 2b. As observed earlier for crystalline proteins (Linden et al. 2011) and in glasses (Siemer et al. 2010), the spectral resolution decreases rather monotonously with temperature. There is no sudden step-like broadening taking place while changing the temperature as is the case when going from 280 to 270 K where the majority of the water freezes in a phase transition as evidenced by the proton spectra of Fig. 2a. As the bulk water freezes, the protein is still surrounded by a rather large amount of mobile water. Upon further lowering of the temperature, the spectral resolution gradually decreases. Even in the region below 220 K, where proton spectra do not indicate any mobile water in the sample, further changes in the spectrum, in particular in the methyl region, are still observed.

To obtain site-specific information on line broadening, 2D DREAM spectra (Verel et al. 2001; Westfeld et al. 2012) were recorded at different temperatures. Figure 4 shows the carbonyl and aliphatic region of a DREAM spectrum of HET-s(218–289) taken at room temperature. The 13 labeled peaks indicate spectrally unambiguous resonances that will be followed in detail below. They were chosen because of their location in the structurally well-defined part and because they can be followed over the

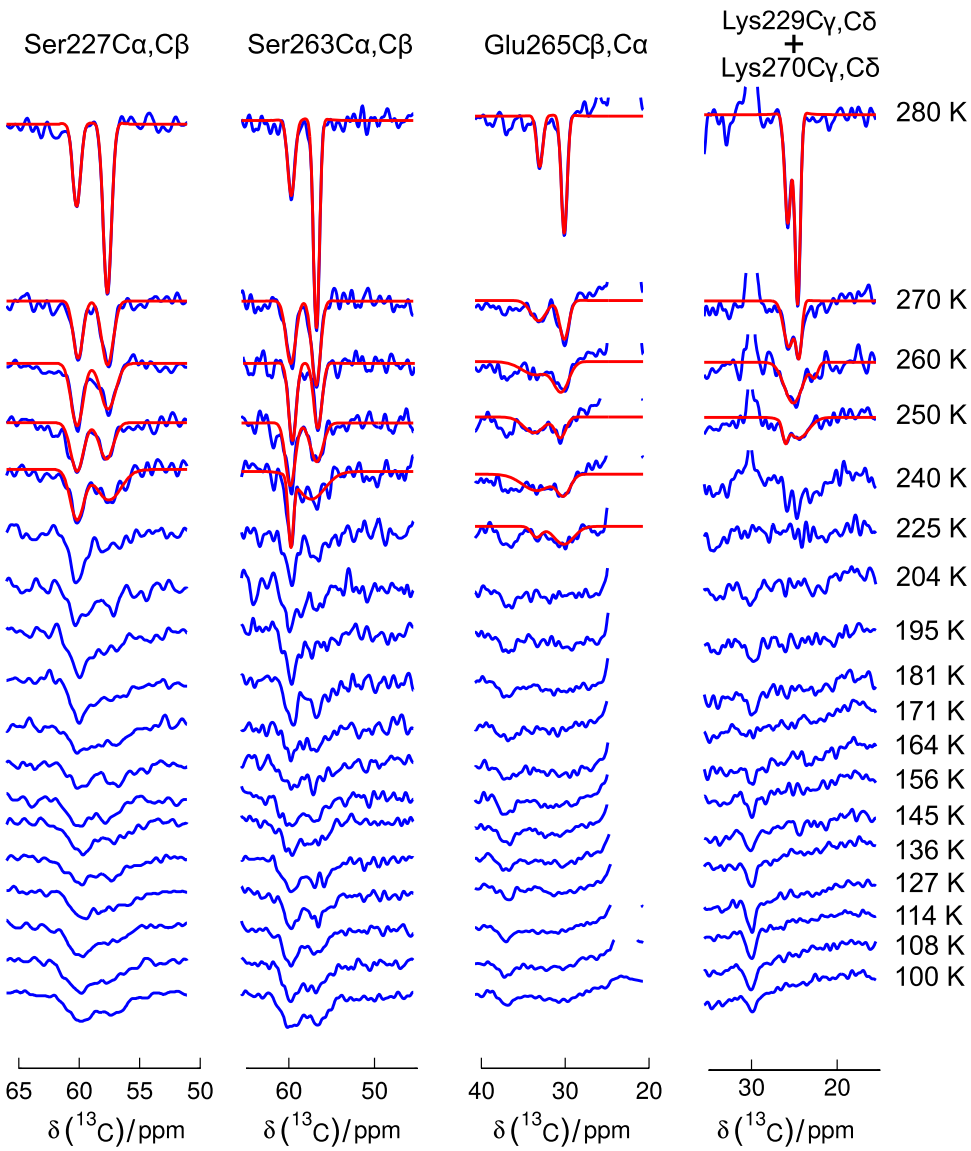

Fig. 7 1D slices from 2D spectra (along direct dimension) are given as *blue lines* the corresponding fits as *red lines*. All residues shown in this Figure point to the outside of the fibril (see Fig. 1) and show a strong line broadening within the first 40 K after freezing. The fits have been omitted where not meaningful anymore

entire temperature range without significant overlap from other crosspeaks (vide infra).

Figure 5 shows examples of HET-s(218–289) DREAM spectra at nine different temperatures between 280 and 100 K. The resolution of the spectrum decreases gradually with lower temperature as already witnessed by the 1D spectrum. Still, until 240 K many resonances can be resolved. It is also evident that different residues react differently to a change in temperature. There is no indicatioon for additional signals (e.g. from the loops found as flexible at room temperature (Siemer et al. 2006; van Melckebeke et al. 2010)) appearing in the low-temperature spectra but they may be hidden by overlap.

1D slices from 2D DREAM spectra for different temperatures are shown in Fig. 6 for Ala228, Ala237, Thr233, Ile231 and Ser273 which point to the inside of the fibril as seen in Fig. 1. We note that these resonances can be observed over the entire temperature range down to 100 K even if they do indeed broaden with decreasing temperature.

Figure 7 shows the 1D slices for residues Ser227, Ser263, Glu265 as well as Lys229 and Lys270 which point to the outside of the fibril. In these cases, the resonances broaden significantly already at the freezing point of the bulk water and almost vanish around 240 K. Indeed the least square fitting procedure has difficulties to find a peak in some of the low temperature data.In these cases, the fit is omitted from the figure.

In Fig. 8 the resonances of Ala247 and 248, which are both located at the start of the flexible loops as well as Gln240, which is located in a semi-hydrophobic pocket (see Fig. 1) are displayed. They show an intermediate broadening behavior between inside and outside residues, more similar to the inside residues though.

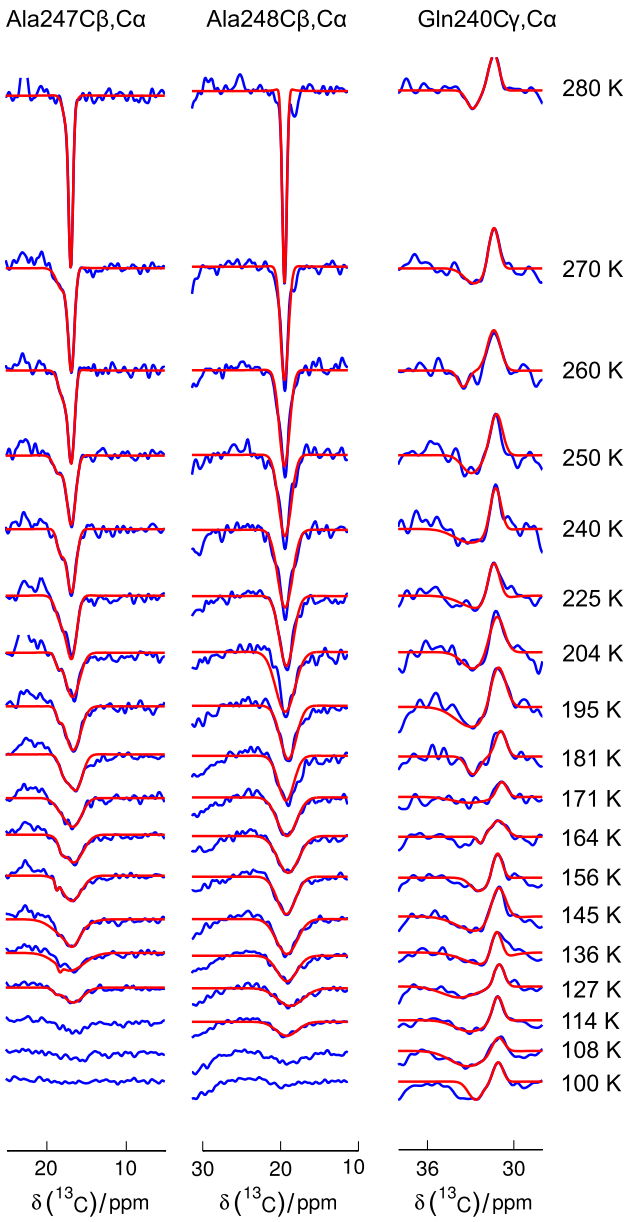

Fig. 8 1D slices from 2D spectra (along direct dimension) given as *blue lines* and best fit as *red lines*. The two alanine residues are located at the beginning of the long loop (see Fig. 1), the glutamine in the hydrophobic pocket formed between the fibril core and the C-terminus. The line width of these residues remains relatively narrow to low temperature. The fits have been omitted where not meaningful anymore

To further quantify these observations, all cross peaks marked in Fig. 3 have been evaluated in terms of line width (FWHH) and peak intensities as obtained by fitting the one-dimensional traces through the cross-peak maxima by a Gaussian function (see red traces in Figs. 6, 7, 8). The results of the fits are displayed in Fig. 9 where the residues are grouped according to their topology into (a) outside residues: Ser227, Lys229, Ser263, Glu265, Lys270, (b) inside

Fig. 9 Line width and peak intensity obtained from the fits in Figs. 6, 7, 8 as a function of temperature grouped according to their topology into **a** outside residues: Ser227, Lys229, Ser263,Glu265,Lys270, **b** inside Residues: Ala228, Ile231, Thr233, Ala237, Ser273, **c** helical-conformation residues at the beginning of the long loop in HET-s(218–289), namely residues Ala247, Ala248 and **d** the hydrophobic pocket residue Gln240. **e** individual broadening behavior illustrated via the schematic illustration the structure of HET-s(218–289). The figure part **f** shows a schematic drawing of the protein surrounded by mobile water and ice after freezing and the successive shrinking of the mobile water layer as it is indicated by the data

Residues: Ala228, Ile231, Thr233, Ala237 and Ser273, (c) helical-conformation residues just before the beginning of the long loop in HET-s(218–289), namely residues Ala247, Ala248 and (d) the hydrophobic pocket residue Gln240. Their position in the structure is also indicated in Fig. 9.

Discussion and conclusion

Categorizing the residues into the groups according to their position in the structure, clear differences are observed:

i. Inside residues: the resonances from residues that point into the core of the fibril broaden comparatively little in the temperature region from 280 to 200 K. For these parts, the resonances remain visible with a line width below 2 ppm down to 140 K, e.g. for Ala228CβCα, or even down to 100 K as for Ala237CβCα. Ser237Cα-Cβ remains visible down to 200 K. At these temperatures no mobile water is detected in the NMR spectrum (Fig. 2a). All the inside residues show little change at the freezing point of the bulk of the solvent water.
ii. Outside residues are all characterized by a significant increase of the line width between 280 K and 270 K where most of the water freezes. Between 230 and 250 K, the line width reaches 2 ppm and the resonances become unobservable. These residues are sensitive to the changes in hydration shell and broaden significantly with the appearance of an ice phase even if there is still liquid water available in the system.
iii. Alanine residues in α-helical conformation before the beginning of the flexible loop. They behave similarly to the inside residues and seem to be shielded from the influence of the surrounding water.
iv. Q240 in the semi-hydrophobic pocket: this resonance does hardly broaden over the entire temperature range observed,

The molecular structure plot in Fig. 9e summarizes the findings for the temperature-dependent broadening behaviors of all residues investigated in detail. Residues with a weak temperature dependence are marked in blue, while residues which exhibit a strong temperature dependence

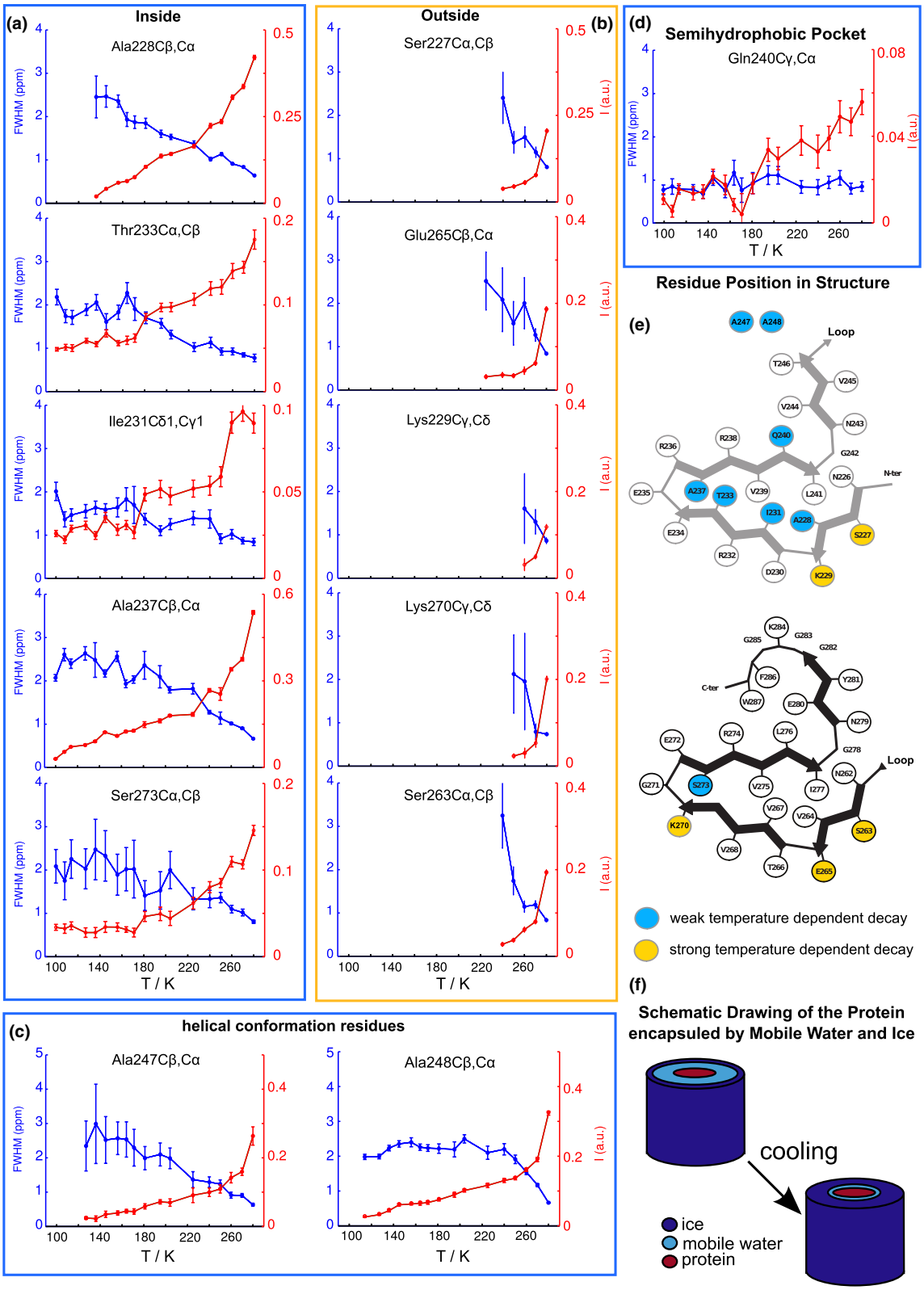

in line width are marked in yellow. It is evident that the temperature-dependent line broadening of individual residue is systematically weaker for non-solvent-exposed residues. This indicates that the initial broadening process is indeed highly influenced by the gradual loss of mobile water around the fibril, which is visualized in the schematic drawing in Fig. 9f by mobile water and ice surrounding the fibril. With decreasing temperature the mobile water layer

diminishes, as indicated in the Fig. 9f. It should be noted that fibrils can bundle and the water may not be evenly distributed. No dry contacts have, however, been found and each fibril is enclosed by water. (van Melckebeke et al. 2011) It is interesting to note that similar broadening of resonances is observed upon lyophilization, and it is tempting to ascribe some aspects of the line broadening in our fibrillar sample as caused by a freeze-drying effect where more and more water is recruited into the ice phase.

Acknowledgements This work has been supported by the Swiss National Science Foundation (Grant 200020_159707 and 200020_146757), the ETH Zurich Research Grant (ETH-08 10-1) and the French ANR (ANR-12-BS08- 0013-01, ANR-14-CE09-0024B).

References

Bajaj VS, van der Wel PCA, Griffin RG (2009) Observation of a low-temperature, dynamically driven structural transition in a polypeptide by solid-state NMR spectroscopy. J Am Chem Soc 131:118–128. doi:10.1021/ja8045926

Balguerie A, Reis Dos S, Ritter C et al (2003) Domain organization and structure–function relationship of the HET-s prion protein of *Podospora anserina*. EMBO J 22:2071–2081

Bayro MJ, Debelouchina GT, Eddy MT et al (2011) Intermolecular structure determination of amyloid fibrils with magic-angle spinning and dynamic nuclear polarization NMR. J Am Chem Soc 133:13967–13974. doi:10.1021/ja203756x

Böckmann A, Gardiennet C, Verel R et al (2009) Characterization of different water pools in solid-state NMR protein samples. J Biomol NMR 45:319–327. doi:10.1007/s10858-009-9374-3

Böckmann A, Ernst M, Meier BH (2015) Spinning proteins, the faster, the better? J Magn Reson 253:71–79. doi:10.1016/j.jmr.2015.01.012

Can TV, Ni QZ, Griffin RG (2015) Mechanisms of dynamic nuclear polarization in insulating solids. J Magn Reson 253:23–35. doi:10.1016/j.jmr.2015.02.005

Colvin MT, Silvers R, Ni QZ et al (2016) Atomic resolution structure of monomorphic Aβ42 amyloid fibrils. J Am Chem Soc 138:9663–9674. doi:10.1021/jacs.6b05129

Debelouchina GT, Bayro MJ, van der Wel PCA et al (2010) Dynamic nuclear polarization-enhanced solid-state NMR spectroscopy of GNNQQNY nanocrystals and amyloid fibrils. Phys Chem Chem Phys 12:5911–5919. doi:10.1039/c003661g

Debelouchina GT, Bayro MJ, Fitzpatrick AW et al (2013) Higher order amyloid fibril structure by MAS NMR and DNP spectroscopy. J Am Chem Soc 135:19237–19247. doi:10.1021/ja409050a

Detken A, Hardy E, Ernst M, Meier BH (2002) Simple and efficient decoupling in magic-angle spinning solid- state NMR: the XiX scheme. Chem Phys Lett 356:298–304

Ernst M, Meier BH (2010) Adiabatic polarization-transfer methods in MAS spectroscopy. eMagRes (EMR) 1–12 doi:10.1002/9780470034590.emrstm0004.pub2

Glass N, Dementhon K (2006) Non-self recognition and programmed cell death in filamentous fungi. Curr Opin Microbiol 9:553–558

Hediger S, Meier BH, Ernst R (1995) Adiabatic passage Hartmann–Hahn cross polarization in NMR under magic angle sample spinning. Chem Phys Lett 240:449

Henzler-Wildman K, Kern D (2007) Dynamic personalities of proteins. Nature 450:964–972. doi:10.1038/nature06522

Lesage A, Böckmann A (2003) Water-protein interactions in microcrystalline Crh measured by H-1-C-13 solid-state NMR spectroscopy. J Am Chem Soc 125:13336–13337. doi:10.1021/ja036720y

Lesage A, Gardiennet C, Loquet A et al (2008) Polarization transfer over the water-protein interface in solids. Angew Chem Int Ed Engl 47:5851–5854. doi:10.1002/anie.200801110

Linden AH, Franks WT, Akbey U et al (2011) Cryogenic temperature effects and resolution upon slow cooling of protein preparations in solid state NMR. J Biomol NMR 51:283–292. doi:10.1007/s10858-011-9535-z

Lu J-X, Qiang W, Yau W-M et al (2013) Molecular structure of beta-amyloid fibrils in alzheimer's disease brain tissue. Cell 154:1257–1268. doi:10.1016/j.cell.2013.08.035

Nagaraj M, Franks TW, Saeidpour S et al (2016) Surface binding of TOTAPOL assists structural investigations of amyloid fibrils by dynamic nuclear polarization NMR spectroscopy. ChemBioChem 17:1308–1311. doi:10.1002/cbic.201600185

Shi C, Fricke P, Lin L, et al (2015) Atomic-resolution structure of cytoskeletal bactofilin by solid-state NMR. Sci Adv 1:e1501087–e1501087. doi:10.1126/sciadv.1501087

Siemer AB, McDermott AE (2008) Solid-state NMR on a Type III antifreeze protein in the presence of Ice. J Am Chem Soc 130:17394–17399. doi:10.1021/ja8047893

Siemer A, Arnold A, Ritter C et al (2006) Observation of highly flexible residues in amyloid fibrils of the HET-s prion. J Am Chem Soc 128:13224–13228

Siemer AB, Huang K-Y, McDermott AE (2010) Protein-ice interaction of an antifreeze protein observed with solid-state NMR. P Natl Acad Sci USA 107:17580–17585. doi:10.1073/pnas.1009369107

Siemer AB, Huang K-Y, McDermott AE (2012) Protein linewidth and solvent dynamics in frozen solution NMR. PLoS ONE 7:e47242. doi:10.1371/journal.pone.0047242

Tekely P, Palmas P, Canet D (1994) Effect of proton spin-exchange on the residual C-13 MAS NMR linewidths - phase-modulated irradiation for Efficient heteronuclear decoupling in rapidly rotating solids. J Magn Reson Ser A 107:129–133

Thurber KR, Tycko R (2009) Measurement of sample temperatures under magic-angle spinning from the chemical shift and spin–lattice relaxation rate of 79Br in KBr powder. J Magn Reson 196:84–87. doi:10.1016/j.jmr.2008.09.019

Tuttle MD, Comellas G, Nieuwkoop AJ et al (2016) Solid-state NMR structure of a pathogenic fibril of full-length human alpha-synuclein. Nat Struct Mol Biol 23:409–415. doi:10.1038/nsmb.3194

van Beek JD, Kummerlen J, Vollrath F, Meier BH (1999) Supercontracted spider dragline silk: a solid-state NMR study of the local structure. Int J Biol Macromol 24:173–178

van Melckebeke H, Wasmer C, Lange A et al (2010) Atomic-resolution three-dimensional structure of HET-s(218–289) amyloid fibrils by solid-state NMR spectroscopy. J Am Chem Soc 132:13765–13775. doi:10.1021/ja104213j

van Melckebeke H, Schanda P, Gath J et al (2011) Probing water accessibility in HET-s(218–289) amyloid fibrils by solid-state NMR. J Mol Biol 405:765–772. doi:10.1016/j.jmb.2010.11.004

Verel R, Ernst M, Meier BH (2001) Adiabatic dipolar recoupling in solid-state NMR: the DREAM scheme. J Magn Reson 150:81–99

Wälti MA, Ravotti F, Arai H et al (2016) Atomic-resolution structure of a disease-relevant Aβ(1–42) amyloid fibril. P Natl Acad Sci USA 113:E4976–E4984. doi:10.1073/pnas.1600749113

Wasmer C, Lange A, van Melckebeke H et al (2008) Amyloid fibrils of the HET-s(218–289) prion form a beta solenoid

with a triangular hydrophobic core. Science 319:1523–1526. doi:10.1126/science.1151839

Westfeld T, Verel R, Ernst M et al (2012) Properties of the DREAM scheme and its optimization for application to proteins. J Biomol NMR 53:103–112. doi:10.1007/s10858-012-9627-4

Wickramasinghe NP, Parthasarathy S, Jones CR et al (2009) Nanomole-scale protein solid-state NMR by breaking intrinsic 1HT1 boundaries. Nat Methods 6:215–218. doi:10.1038/nmeth.1300

Saupe SJ (2011) The [Het-s] prion of *Podospora anserina* and its role in heterokaryon incompatibility. Seminars in cell developmental biology. vol 22. Academic Press, London 460–468. doi:10.1016/j.semcdb.2011.02.019